



Synthesis, Characterization and Evaluation of Anti-bacterial, Anti-parasitic and Anti-cancer Activities of Aluminum-Doped Zinc Oxide Nanoparticles

Khawla S. Khashan¹ · Ghassan M. Sulaiman² · Sura A. Hussain¹ · Thorria R. Marzoog² · Majid S. Jabir²

Received: 3 February 2020 / Accepted: 24 March 2020 / Published online: 29 March 2020
© Springer Science+Business Media, LLC, part of Springer Nature 2020

Abstract

The preparation of nanoparticles by utilizing laser ablation in liquid has gained extensive attention as a reliable, simple, fast, efficient and environmental friendly method. In the present study, zinc oxide nanoparticles (ZNO NPs) and aluminum-doped ZNO nanoparticles (Al ZNO NPs) were produced via laser ablation in deionized water. The synthesized nanoparticles were characterized by X-ray diffraction (XRD), UV–Vis spectroscopy, field emission scanning electron microscopy (FESEM) and energy dispersive spectrum (EDS) analyses. ZNO NPs showed that the particle size increased with the increase in the number of laser pulses, while the shape changed from nanoplate to nanowire, along with the presence of small agglomerated spherical nanoparticles. The results confirmed the formation of Al ZNO NPs with Wurtzite hexagonal phase where the shape being modified from nanowire to spherical, along with high agglomeration. The EDS analysis showed that all peaks had conformity with the peaks of Zn, O, and Al atoms, with no impurities. The antibacterial activity test revealed a largest inhibition zone in *Staphylococcus aureus* as compared to *Escherichia coli*, with a more potent effect for Al ZNO NPs when compared with ZNO NPs alone. The same effects were recorded against *Leishmania tropica* and *L. donovani*, with stronger activity against the former parasite. The nanoparticles also showed anticancer activities against MDA-MB-231 cells, suggesting that cancer cells were targeted by the NPs through induction of cell death. Consequently, these investigations reveal that the prepared particles may be useful for the development of anti-cancer drugs, including those used for breast cancer therapy.

Keywords Laser ablation · Al ZNO NPs · Anti-bacterial · Anti-leishmanial · MDA-MB-231

1 Introduction

Metal oxides received an increasing interest in research due to low cost, nontoxicity, simple processing steps, and beneficial applicability in many fields for electronic, optoelectronic and biological labeling and catalysis [1–3]. Their unique properties depend on both the size and the morphology of nanoparticles [4]. There is a large variety of metal oxide nanomaterials such as nanoparticles, nanowires, nanotubes, and nanoporous structures. Hussein et al. prepared

fluorescent quantum dots and studies their properties [5]. Khashan et al. synthesized InN NPs by Nd:YAG laser ablation of indium target submerged under ammonium hydroxide and examined their characterization [6]. Singh et al. successfully synthesized (2–6 nm) spherical monoclinic structured of CuO NPs with an optical band gap of 2.5 eV via green method using *P. guajava* leaf extract [7].

Zinc oxide (ZNO) is one of the promising nanomaterials that is prepared in different methods and used in a wide range of applications, including optoelectronic devices, energy storage and biomedical sciences [8–10]. ZNO NPs received increasing attention in recent years, not only because their stability under harsh processing conditions, but also because they are generally regarded as safe materials to human beings and animals. Metal oxide nanoparticles with varying physicochemical characteristics can exhibit different antibacterial mechanisms and effects [11]. The benefits of utilizing ZNO as an antibacterial agent are derived from the properties of Zn as a mineral that is essential to humans, non-toxic, long-term

✉ Ghassan M. Sulaiman
gmsbiotech@hotmail.com; 100135@uotechnology.edu.iq

¹ Division of Laser Science and Technology, Department of Applied Sciences, University of Technology, Baghdad, Iraq

² Division of Biotechnology, Department of Applied Science, University of Technology, Baghdad, Iraq

stable and strongly active even when administrated at lower concentrations [12]. Oxide nanoparticles with a combination of two or three metals can be developed for efficient elimination of various bacterial strains, even those highly resistant to traditional treatments. The activity of ZNO NPs can be enhanced by doping with different metals such as Mn, Al, Mg, In, Cd and Ti [13–16]. Al is considered as a suitable choice for dopant materials in terms of its availability and non-toxicity [17].

To date, many techniques have been used to synthesize ZNO NPs with different shapes and sizes, such as the hydrothermal [18], chemical [19], and green synthesis methods [20]. Most of these techniques involve adding a source of Al in order to achieve Al-doped ZNO nanoparticles (Al ZNO NPs). Also, Saxena et al. have systematically designed Al ZNO NPs via a co-precipitation method, and evaluate the antibacterial properties against *Escherichia coli* and *E. hirae* [12]. Bhuiyan et al. reported that Al ZNO nanostructure have been successfully grown by an electrochemical method [21]. Singh et al. successfully synthesized spherical, polydispersity of ZNO NPs with average size of 20 nm via a green synthesis method using an aqueous leaf extract of *Punica granatum* [22].

However, one of the simplest methods for preparing nanoparticles can be the utilizing of laser ablation in liquid (LAL). This method is based on the process of pulse laser ablation of a metallic target that is immersed in liquid. This method is preferred because it is simple, fast, efficient and environmental friendly. It is used to synthesize a wide range of NPs colloidal solutions for various types of materials in many type of liquids. Therefore, this process could be utilized to synthesize different types of materials with various shapes of nanoparticles [23–25]. Furthermore, it can be used to reduce the size of initial particles in liquid and to reshape and de-agglomerate the nanoparticles [26]. In general, nanosized materials produced by LAL technique have a great importance in recent years because of their interesting properties and their efficient applications in different fields, including biomedical uses [27, 28]. Until now, only limited information is available on the potential toxicity of Al ZNO NPs to bacterial species, parasites and cancer cells. Thus, the present research is aiming at the synthesis of Al ZNO NPs colloidal suspension by LAL and studying their properties against two clinical isolates of bacteria, two species of leishmania, and human triple-negative breast cancer (MDA-MB-231) cells.

2 Experimental Work

2.1 Materials

Zinc target (99.999%) was purchased from Sigma–Aldrich, Saint Louis, USA. Aluminum target (99.999%) were

purchased from Himedia Ltd., Mumbai, India. Mueller Hinton agar and nutrient broth were purchased from Merck, Germany. Tissue culture plastic wares were obtained from BD Bioscience, USA. RPMI 1640, fetal calf serum (FCS) 2,2-diphenyl-1-picrylhydrazyl (DPPH), 3-(4,5-dimethylthiazal-z-yl)-2, 5-diphenylterazolium (MTT) and crystal violet stain were purchased from Sigma Chemical Co., USA. The antibiotics penicillin–streptomycin were purchased from Biosource International, Nivelles, Belgium. All other chemicals and reagents were used at analytical grade. Water was double distilled with Millipore water purification system.

2.2 Organisms

Two clinical isolates like *Escherichia coli* (gram-negative) and *Staphylococcus aureus* (gram-positive) were used to evaluate the antibacterial activity of prepared nanoparticles. The clinical isolates were obtained from patients admitted to several Iraqi medical centers in Baghdad. *E. coli* were isolated from patients suffering from urinary tract infections. While, *S. aureus* were isolated from patients with wound infections. The isolates were processed and identified by standard biochemical methods at Medical Microbiology Laboratory, Biotechnology Division, Department of Applied Science, University of Technology, Baghdad, Iraq. Two species of Leishmania (*L. tropica* and *L. donovani*) were kindly donated by Dr. Mohammad M.F. Al-Halbosiy (Biotechnology Research Center, AL-Nahrain University, Baghdad, Iraq). Parasites were cultured in RPMI-1640 medium with L-glutamine supplemented with FCS (10%). Parasites were passaged weekly by transferring 3×10^5 promastigotes from a previous culture to 5 mL of RPMI-1640 plus FCS medium (10%). The cultivation of human triple-negative breast cancer (MDA-MB-231) cells was maintained in RPMI-1640 cell culture medium mixed with HEPES (20 mM) as a buffering medium and with FCS (5%), L-glutamine (2 mM), sodium pyruvate (10 mM) and both penicillin and streptomycin (100 IU mL^{-1}). The mixture was kept in tissue culture flasks ($T 25 \text{ cm}^2$; Falcon, USA) with a humidified atmosphere and optimal conditions ($37 \text{ }^\circ\text{C}$, 5% CO_2) to retain the weekly-passaged cells in the logarithmic phase of growth.

2.3 Preparation of ZNO and Al ZNO Nanoparticles

High intense pulsed Neodymium-doped Yttrium Aluminium Garnet (Nd:YAG) laser system (HUAFEI, China) providing pulses of 1064 nm wavelength with maximum energy per pulse of 1000 mJ, 9 ns pulse width, repetition rate of 1 Hz and effective beam diameter of 5 mm, was used for preparing the nanoparticles. The reaction condition was performed at ambient room temperature and the schematic representation for synthesis of ZNO and Al ZNO NPs is illustrated in Fig. 1. In brief, Nd:YAG laser

was applied to irradiate the surface of the zinc target that was immersed in 3 mL of deionized distilled water (DIW) contained in a small glass vessel with continuous spinning. The height of water above the target was 2 mm, while the laser beam was focused at the surface of the target by a convex lens with a focal length of 100 mm and focus energy at 700 mJ, and different numbers of pulses (25, 50, 75, 100 and 125). By interaction between laser pulses and the solid target in liquid environment, target ablation was achieved and the required nanomaterial was obtained as a suspension. At a constant concentration of zinc oxide nanoparticles, the doping occurred by replacing zinc target with aluminum target and hitting the surface of the aluminum target with constant laser energy and different numbers of pulses (20, 30, 40, 50).

The concentration of the prepared NPs was prepared by utilizing a four digits-balances to weigh the target before the ablation process. After ablation with a number of pulses, the target was dried and weighed again. The amount of the target mass that was ablated (ΔM) could be found by the following equation:

$$\Delta M (\Delta g) = m_1 - m_2 \quad (1)$$

where m_1 = target mass before ablation; m_2 = target mass after ablation.

Then, mass concentration was calculated via dividing the difference (ΔM) by the liquid volume:

$$\text{Mass concentration } (\mu\text{g mL}^{-1}) = \Delta M / \text{liquid volume} \quad (2)$$

The doping ratio (DR %) of aluminum could be calculated by dividing mass concentration of (Al) NPs by the total composition.

$$\text{DR (\%)} = \frac{\text{M.C (AlO)}}{\text{M.C (AlO + ZNO)}} \quad (3)$$

The prepared NPs with their respective concentrations, doping ratios, and the used number of pulses are listed in Table 1.

2.4 Characterization of ZNO and Al ZNO Nanoparticles

X-ray diffraction (XRD) data were obtained using Philips PW (Japan) XRD with Cu-K α radiance source at 2θ angle = (10° to 80° with scan speed 5.0000 (° min⁻¹)). Double beam UV-Vis spectrophotometer (SP-3000 Plus model, Optima, Tokyo, Japan) was used to measure the optical absorption spectra of ZNO and Al ZNO NPs suspension with different concentrations at a spectral range of 200–900 nm. These steps were performed at room

Fig. 1 The schematic representation for synthesis of ZNO and Al ZNO NPs

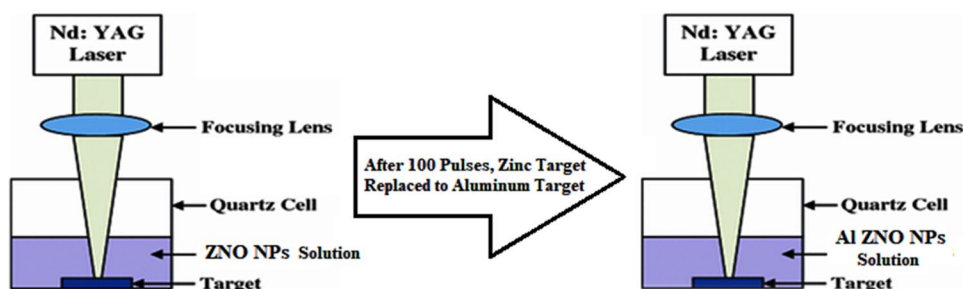


Table 1 Samples of NPs with their respective concentrations, doping ratios, and the used number of pulses

Sample code	Sample	Sample abbreviation	Number of pulses	Mass concentration ($\mu\text{g mL}^{-1}$)
A	Control ^a	–	–	–
B	1	ZNO	25	66.6
C	2	ZNO	50	133.3
D	3	ZNO	75	200
E	4	ZNO	100	266.6
F	5	ZNO	125	333.3
G	Al 1	Al ZNO	20	0.2% doping ratio
H	Al 2	Al ZNO	30	0.27% doping ratio
I	Al 3	Al ZNO	40	0.33% doping ratio
J	Al 4	Al ZNO	50	0.42% doping ratio

^aControl: deionized distilled water

temperature in a 1 cm optical path using quartzite cell. Field emission scanning electron microscopic (FESEM) analysis was conducted using MIRA 3 TESCAN (Brno, Czech Republic) operating with 10 keV voltage to provide data on the distribution of particle shape and size of ZNO and Al ZNO NPs. Energy dispersive spectrum (EDS) analysis gives a chemical composition of the nanomaterial synthesis by using Inspect S50 scanning electron microscope (FEI, Eindhoven, Netherlands).

2.5 Antibacterial Activity Assay of ZNO and Al ZNO Nanoparticles

Antibacterial activity of ZNO and Al ZNO NPs suspension was examined against *E. coli* and *S. aureus*. The stock cultures for these two bacterial isolates was transferred into Mueller Hinton agar medium, incubated over night at 37 °C, and stored in refrigerator at 4 °C until used.

2.5.1 Mueller Hinton Agar Preparation

Mueller Hinton Agar was made to reveal antibacterial effectiveness. According to the manufacturer's guidelines, the agar media was prepared by dissolving 28 g of the powder in 1000 mL of deionized distilled water with the assistance of heating and continuous shaking. After autoclaving at 121 °C for 15 min, the agar preparation was cooled at 47 °C by cold water, and solidified in Petri dishes which were left about 15 min till they were cooled at room temperature.

2.5.2 McFarland Solution Preparation

The solution of McFarland was prepared using BaCl₂·0.2H₂O (0.05 mL, 1.175%) and H₂SO₄ (9.95 mL, 1%). The standard solution that symbolized to 5 × 10⁷ bacterial cells per milliliter was compared with turbidity bacterial suspension, which combined and make sure from its suspending. McFarland Suspension was tightly closed to avoid evaporation and wind while covered with foil of aluminum to keep away from light.

2.5.3 Antibacterial Activity of ZNO and Al ZNO NPs by Liquid Medium Method

The antibacterial affectivity of ZNO and Al ZNO nanoparticles was tested against *S. aureus* and *E. coli* via the dilution method in normal saline. To prepare bacterial suspension, bacteria strains were recruited from stored bacterial cultures via a loop, dissolved in normal saline, and calibrated with 0.5 McFarland turbidity standard (5 × 10⁷ cell mL⁻¹).

Both bacterial strains were diluted in normal saline. The dilution method was performed by adding 0.1 mL of nanoparticles suspension for all concentrations of pure ZNO and Al

ZNO NPs to tubes containing 0.9 mL of normal saline inoculated with either bacterial strain. The tubes were placed in an incubator for 3 h, followed by measuring the optical density by spectrophotometer and then the inhibition rate for ZNO and Al ZNO NPs. Curves of optical density represented numbers of viable bacterial cells in normal saline after treatment with ZNO and Al ZNO NPs suspension. The inhibition rate (%) was determined by applying the readings from the UV-spectrophotometer (APEL, PD-303, Japan) in the following equation [23]:

$$\text{Inhibition rate\%} = \frac{\text{Control}(OD) - \text{Test}(OD)}{\text{Control}(OD)} \times 100\%$$

2.5.4 Antibacterial Activity Test of ZNO and Al ZNO NPs by Well Diffusion Method

Antibacterial activity of ZNO and Al ZNO NPs against *E. coli* and *S. aureus* was also measured by the well diffusion method. The bacteria were separated at the surface of Mueller Hinton agar plates. Wells with diameters of about 6 mm were made at the surface of agar media by tips of micropipette, then NPs suspensions with different concentrations were added into the wells. These plates were kept at the incubator for 24 h. The antibacterial effectiveness of nanoparticles was recorded by measuring inhibition zone diameters from different directions using a ruler more than once.

2.6 Anti-parasitic and Anti-cancer Activities of ZNO and Al ZNO NPs by MTT Assay

The cytotoxic activities against two species of *Leishmania* (*L. tropica* and *L. donovani*) as well as against MDA-MB-231 cancer cells were assessed after 24 h using the colorimetric MTT reduction assay [29, 30]. Briefly, culture plates (96-well, flat-bottom; Falcon, USA) were used to seed the cells (200 μL, 1 × 10⁶ mL⁻¹), which were initially kept in the exponential phase of growth for 48 h and then exposed to different concentration of either ZNO or Al ZNO NPs. Following 24 h of incubation, the cells were labeled with MTT in PBS (100 μL, 20 min, 37 °C). After a washing step with tap water, the stain was dissolved by the addition of DMSO (100 mL) and the air bubbles were cleared out through 10 min of incubation. The absorbance (600 nm) was determined using a microplate reader (ELx 800, Bio-Tek Instruments, USA). The percentage of the growth inhibition rate was measured depending on the following equation:

$$\text{Growth inhibition\%} = \frac{\text{Control}(OD) - \text{Test}(OD)}{\text{Control}(OD)} \times 100\%$$

2.7 Statistical Analysis

The statistical analysis was implemented using SPSS package by one-way analysis of variance (ANOVA). Significance of differences was set at $p \leq 0.05$. All measurements were replicated more than three times for each experiment.

3 Results and Discussion

Figure 2 shows the influence of increasing the number of pulses on the nanoparticle concentration for ZNO and Al ZNO NPs prepared by Nd-YAG laser ablation in DIW. The absorbance was taken at a wavelength of 1064 nm and output energy of 700 mJ. The concentration was calculated using Eqs. 1 and 2 as described in Sect. 2.3. The linear relationship between number of pulses and mass concentration explains the gradual increase in number of both ZNO and Al ZNO NPs at liquid suspension with growing number of pulses. This may be related with the increased evaporation in target surface at increased surface heating caused by the increase in number of pulses. In general, production rate of

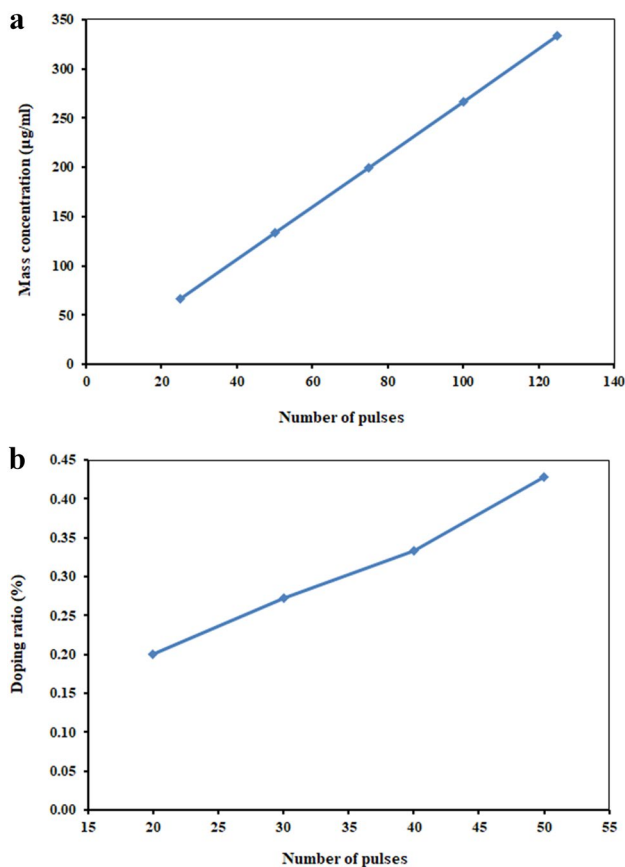


Fig. 2 Mass concentration as a function of number of laser pulses for **a** ZNO NPs and **b** Al ZNO NPs

nanoparticles is dependent on parameters related to optical and thermal properties of the target material, such as surface reflectivity, heat capacity, thermal conductivity, absorbance of light, boiling temperature and enthalpy of vaporization [31]. Number of laser pulses is the most important factor that can influence the efficiency of ablation by affecting the concentration and morphology of nanoparticles released in the liquid; increasing the number of laser pulses leads to an increase in the concentration of nanoparticles. Moreover, size and shape of nanoparticles can be modified by further interaction with laser pulses [32].

Figure 3 shows the XRD patterns for pure ZNO NPs prepared by laser ablation in DIW at 700 mJ with different number of pulses. These spectra exhibited peaks equal to $2\theta = (31.73^\circ, 33.5^\circ, 36.69^\circ, 56.69^\circ, 66.4^\circ, 67.6^\circ, 69^\circ)$ which correspond to the planes of (100), (002), (101), (110), (200), (112), and (201). All samples of ZNO NPs were well matched with the standard card of JCPDS (No. 36–1451), which shows that the ZNO NPs belong to the hexagonal Wurtzite structure. While, the peak at a diffraction angle $\approx 43.76^\circ$ corresponded to (101) plane for Zn^{2+} structures and was matched with the standard card of JCPDS (No. 04–0831). These findings providing an evidence for high activity of the zinc target to generate ZNO nanomaterial suspension in liquid when reacting with water and oxygen molecules [33–35].

Figure 4 shows the XRD results for Al ZNO NPs which exhibited peaks of $2\theta = 43.79^\circ$, corresponding with Miller indices equal to 320 which provides an evidence of the production of Al ZNO NPs inside the suspension and refers to a hexagonal structure of the Al ZNO NPs [28]. Other peaks appeared at $2\theta = 20^\circ, 24^\circ, 25^\circ, 26.6^\circ, 27^\circ, 31.5^\circ, 34.5^\circ, 36.2^\circ$ and 56.6° , corresponding to Miller indices of 111, 112, 004, 100, 013, 020, 014, -214 and 107, respectively. These indices were well matched with the standard cards of JCPDS (No. 36–1451), and (No. 023–1491). These peaks reflected changes according to Al doping ratio, which confirmed the hexagonal structure of Al ZNO NPs nanostructures. All these results are in a good agreement with previously published data [36]. Peaks of Al ZNO NPs tend to shift at a diffraction angle smaller than that for ZNO NPs after increasing Al concentration in ZNO lattice, which is possibly due to the small ionic radius of Al^{3+} [37]. Also, the intensity of diffraction peaks decreases as compared with the intensity of ZnO, indicating that the crystal size decreases when Al incorporates with the ZNO lattice [36].

Figure 5a shows the UV–Vis spectra for ZNO NPs prepared by the laser ablation of zinc target in DIW, achieved at output energy of 700 mJ with different number of pulses. All peaks for these five samples were still within the UV range and centered at approximately 260 nm. Increasing the number of laser pulses caused an increase in the peak of absorbance intensity, possibly due to the increase in the amount of

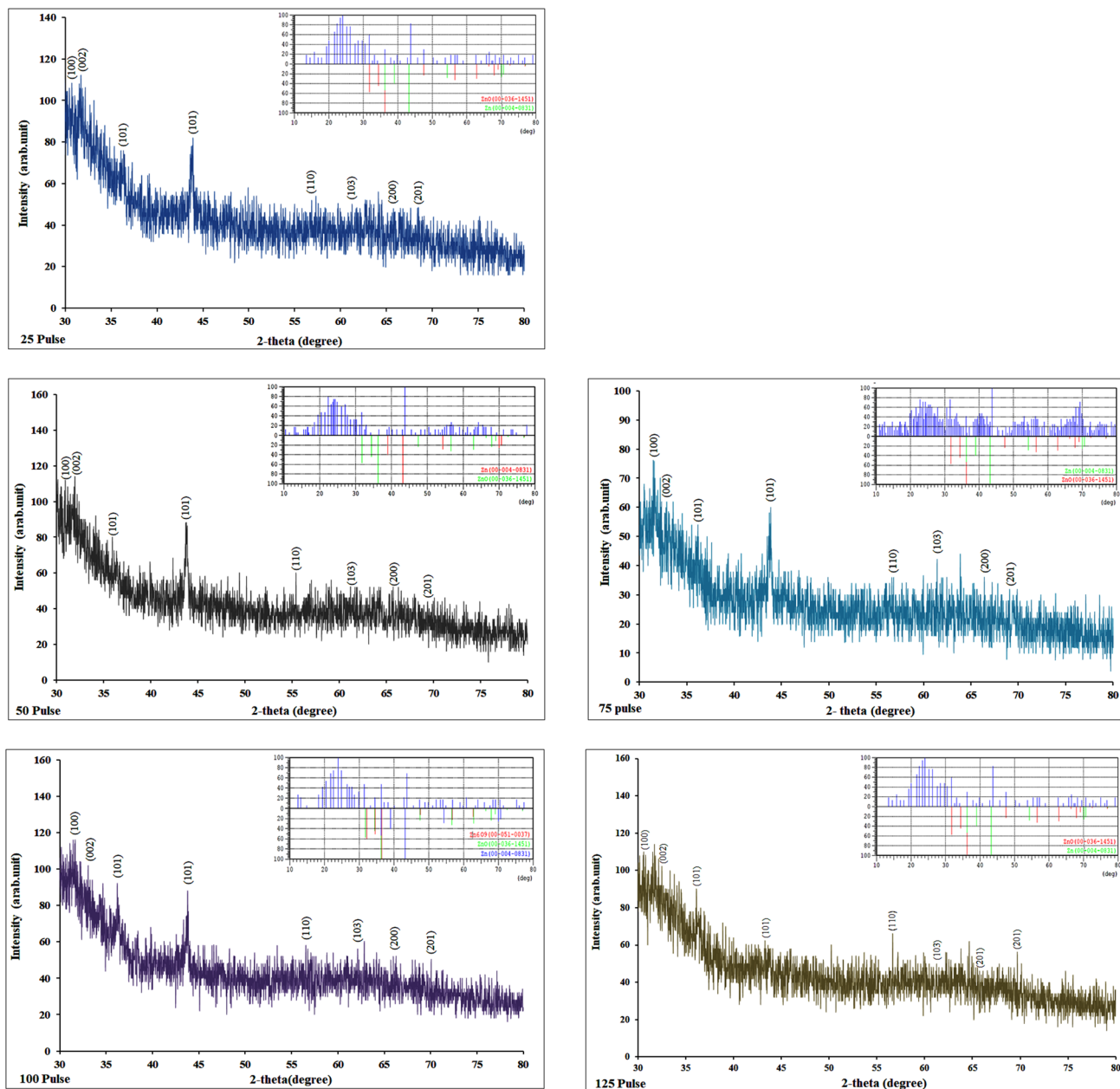


Fig. 3 X-ray diffraction patterns for ZnO NPs with different number of pulses

masses produced by the ablation process inside the colloidal suspension which indicates increasing the concentration of NPs. Also, changing the number of pulses may change the quality of nanoparticles; these particles intercept the path of the laser beam, causing absorption of laser energy which, in turn, results in the reduction in the size of NPs [38]. There were also long tails toward the higher wave length, either because of the scattering rate of particle size or the Urbach effect resulting from the inter-grain depletion regions [39].

Figure 5b demonstrates the UV–visible absorption spectra for Al ZnO NPs prepared at same laser energy with

different doping ratios. All peaks were centered at 260 nm, a position for a UV region of a high absorption edge which was blue-shifted toward shorter wavelength and high energy because of the reduction in particle size by doping Zinc oxide with Al^{3+} . This shift is attributed to the increase in aluminum concentration with increasing the number of laser pulses [40]. From Fig. 5b, it can be observed that the breadth of the absorption region increases with increasing the doping ratio of Al ZnO NPs, indicating that the absorption was caused by the endings of localized levels within the energy gap produced from the change in crystal structure acquired

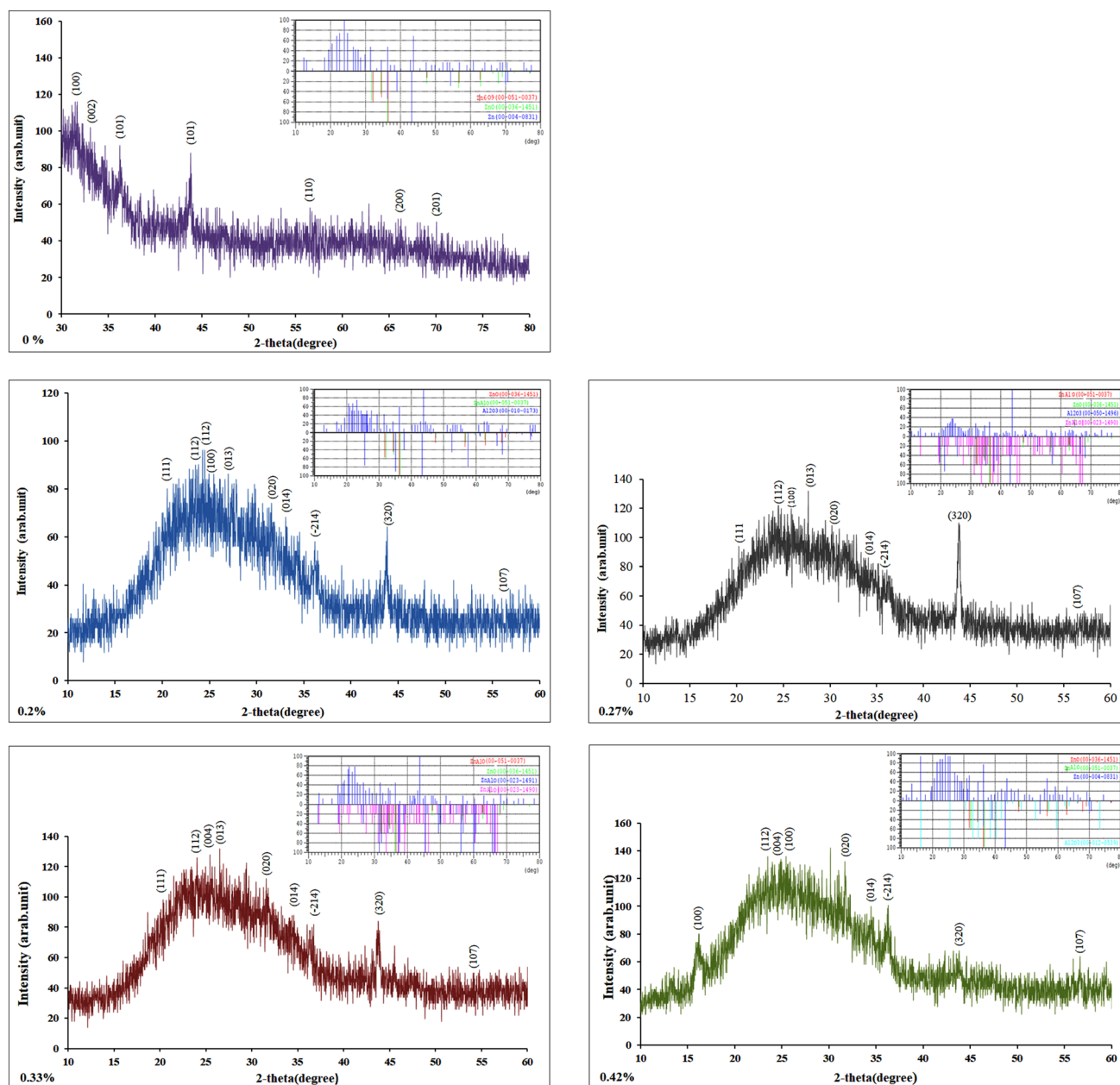


Fig. 4 X-ray diffraction patterns for Al ZNO NPs with different concentrations

by different Al NPs [36]. Also, all peaks in the figure were positioned between the low absorbance at the visible region and the high absorbance at the UV region. In general, the absorbance increases linearly with the doping ratio, which is clear when the absorbance peaks at the 0.27% are slightly higher than those at the 0.2% sample and the absorbance peaks at 0.42% are higher than those at 0.33% samples. However, the absorbance of the former two samples was higher than that of the latter ones, which might be attributed to the scattering by the nanoparticles or the characteristics of aluminum reflectance, since aluminum has a high reflectivity

in the UV region [40, 41]. The variation of band gap for prepared samples can be estimated from transmittance data as seen in Table 2 and these results were in good agreement with previous results of Khan and his co-workers [42].

Figure 6 illustrates the FESEM images for ZNO NPs synthesized by laser ablation at output energy of 700 mJ as with different number of pulses (25, 50, 75, 100, and 125) with their Energy-Dispersive Spectroscopy (EDS) analyses. In general, the morphology of the colloidal preparation changed according to the number of laser pulses. As can be observed, the formed nanoparticles were in the shape of

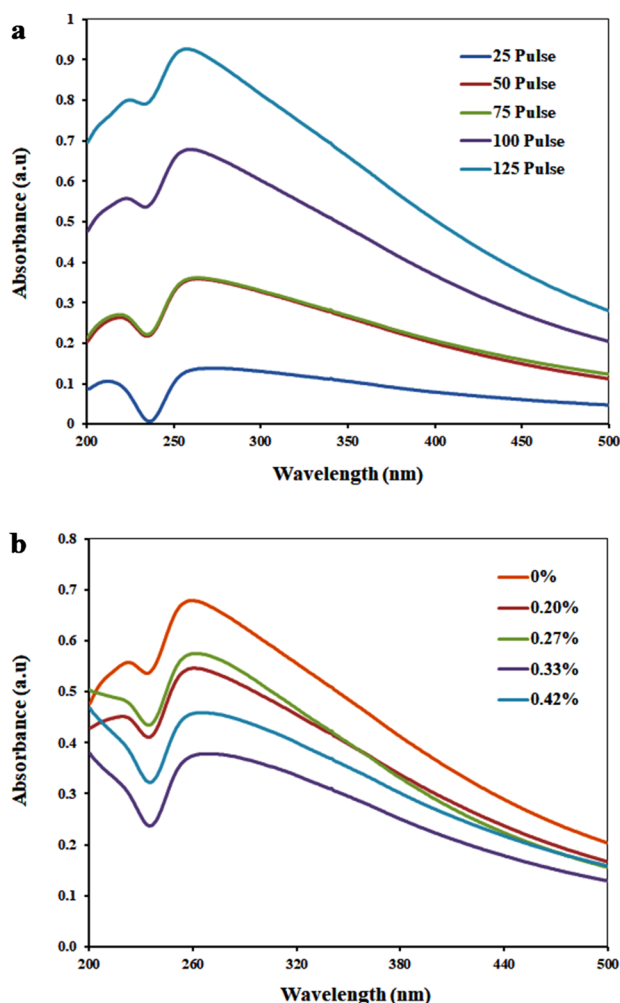


Fig. 5 UV–Vis spectra of **a** ZNO NPs and **b** Al ZNO NPs with five different numbers of pulses

Table 2 Variation of the energy band gap for ZNO NPs and Al ZNO NPs

ZNO NPs		Al ZNO NPs	
Number of pulses	E _g (e.v) ^a	Doping ratio	E _g (e.v)
25	3.05	0	3.20
50	3.10	0.2	3.25
75	3.15	0.27%	3.30
100	3.20	0.33%	3.35
125	3.25	0.42%	3.15

^aE_g (e.v): Band gap energy per electron volt

nanoplate or flakes with a thickness of about 10–50 nm at 25 pulses with average particles diameter was about 44 nm. This structure was modified to a hexagonal-rod shape at 50 pulses, followed by remarkable morphological change

to spherical particles at 75 pulses, with parallel diameter changes from 24 to 42 nm and the average size was about 35 nm. At 100 laser pulses, agglomerates of mostly spherical particles as well as flakes could be clearly observed, with diameter change from 34 to 69 nm and average size was about 50 nm. Nanowires and tiny agglomerates of spherical nanoparticles were observed at 125 pulses. The nanowires were with diameters of about 30 nm whereas the particles had diameters ranging from 22 to 31 nm and average size was about 27 nm. Also, Fig. 6 demonstrates the results of the EDS analysis for ZNO NPs with different number of pulses, indicating the presence of only Zn metal and Oxygen.

Figure 7 shows the FESEM images for Al ZNO NPs at different concentrations. It can be initially observed that the average particle diameters decreased with increasing aluminum concentration [43]. At 0.2% Al, the morphology of the sample resembled a nanowire structure with 28 nm in thickness as well as irregular particles with diameters of about 16–27 nm and average size was about 25 nm. At 0.27% Al, the morphology was changed to a hexagonal nano-rod shape with a diameter of about 126 nm and a thickness of about 88–95 nm and particles with average size was about 82 nm. The morphology kept similar structure with few spherical particles as doping ratio increased to 0.33% Al. Using this ratio, thickness of the nanorod was decreased to 56–64 nm and the diameter of the spherical particles were in the range of 18–22 nm and average size was about 46 nm. Finally, the structure was modified to spherical particles with high aggregation and a diameter of about 22–32 nm and average size was about 27 nm. These results are in full agreement with previously reported data [40, 41]. EDS spectra in Fig. 7 show peaks that well are conformed with those of Zn, O, and Al atoms. No other peaks related to impurities were recorded, clearly explaining that the observed Al ZNO NPs were synthesized from Zn, O and Al elements [44].

Figure 8 shows the optical density and inhibition rate of the culture growth of Gram positive and Gram negative bacteria, in the presence of both pure zinc oxide and Al-doped zinc oxide nanoparticles. UV–Vis spectroscopy, set at 600 nm wavelength, was used to measure the optical density of bacteria in liquid medium. As shown in Fig. 8a, the optical density of *E. coli* was slightly dropped after treatment with ZNO, reaching to a minimum suppression at a concentration 200 μg mL⁻¹. After doping with alumina, the Al ZNO NPs gradually reduced the bacterial culture growth with increasing NPs concentration. The antibacterial effects of ZNO NPs and Al ZNO NPs against *S. aureus* were more effective than that recorded in *E. coli* (Fig. 8a).

Figure 8b shows the inhibition rates for *E. coli* and *S. aureus*, respectively. The blue line indicates the inhibition rate for *E. coli* which began to increase with increasing NPs concentrations, until reaching an inhibition of 28.57% at the third concentration (200 μg mL⁻¹). Less

Fig. 6 FESEM imaging with EDS analysis for five samples of the prepared ZNO NPs with different numbers of pulses

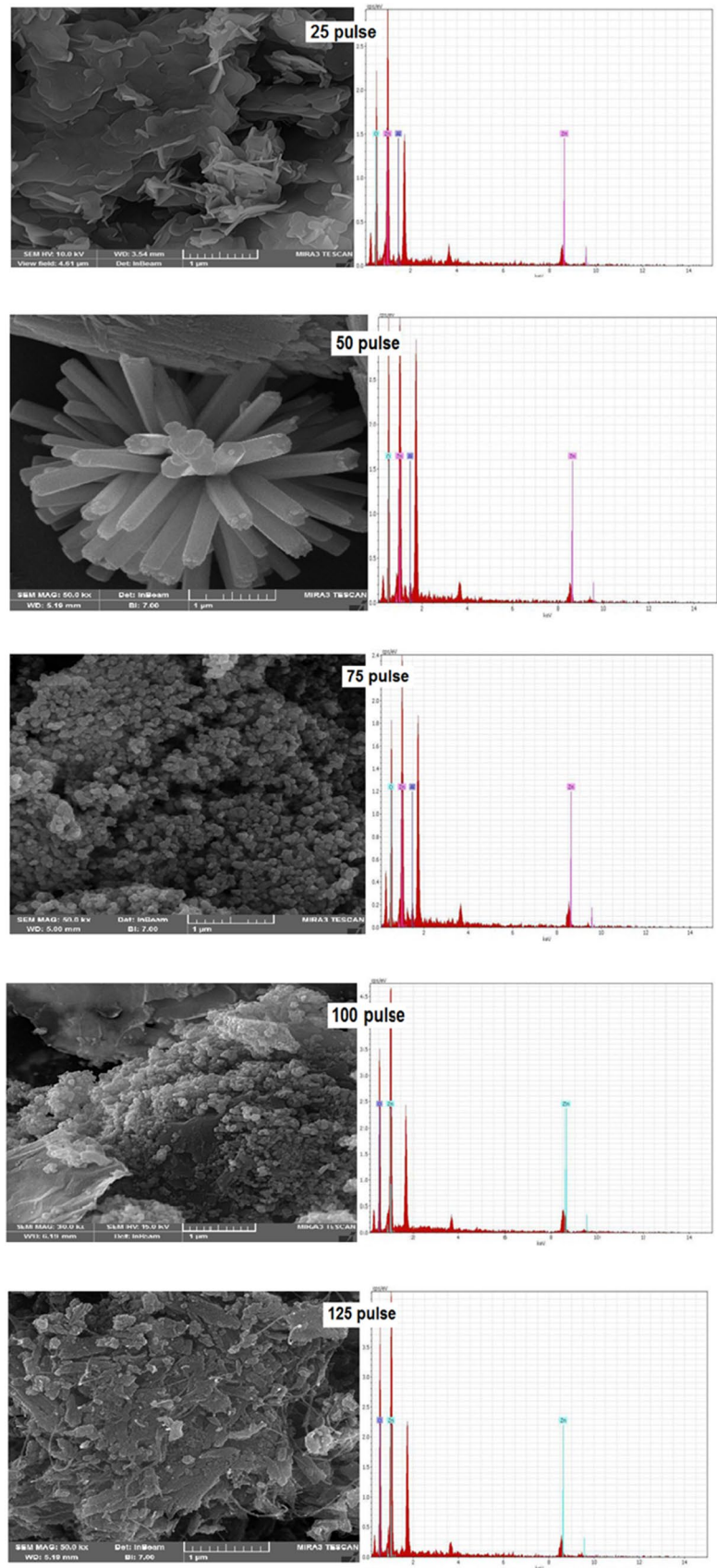
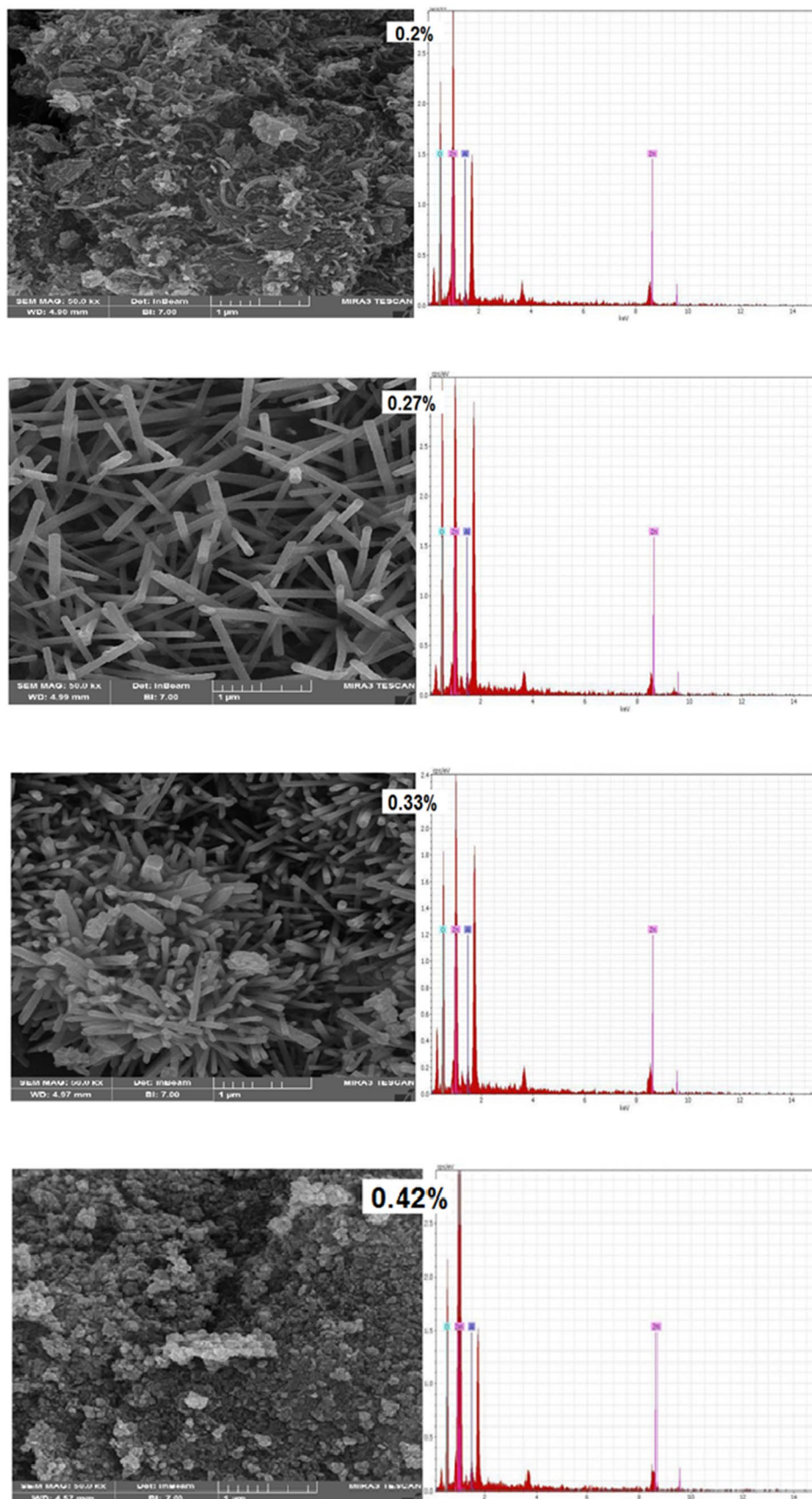


Fig. 7 FESEM imaging with EDS analysis for the prepared Al ZNO NPs with different doping ratios



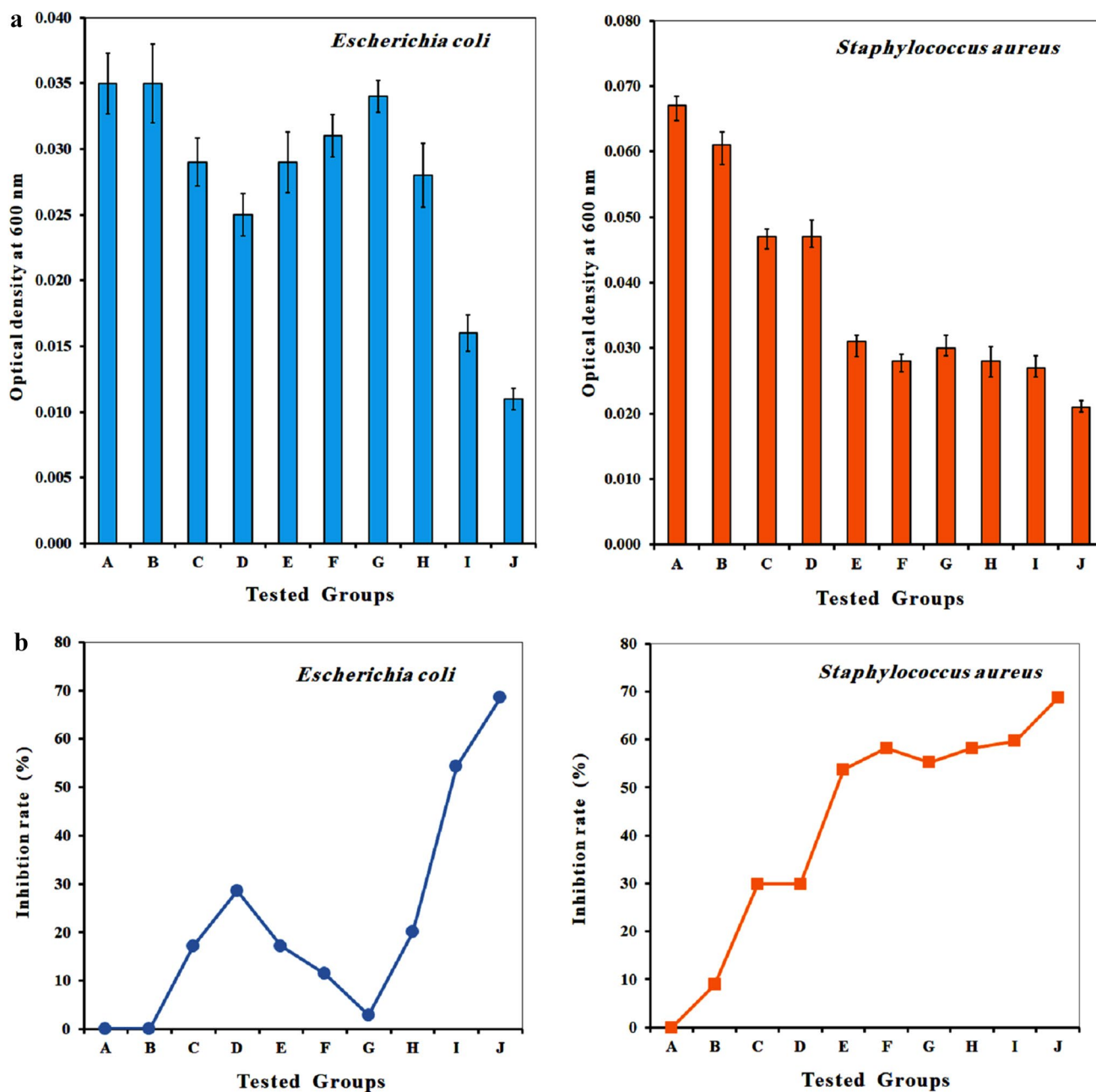


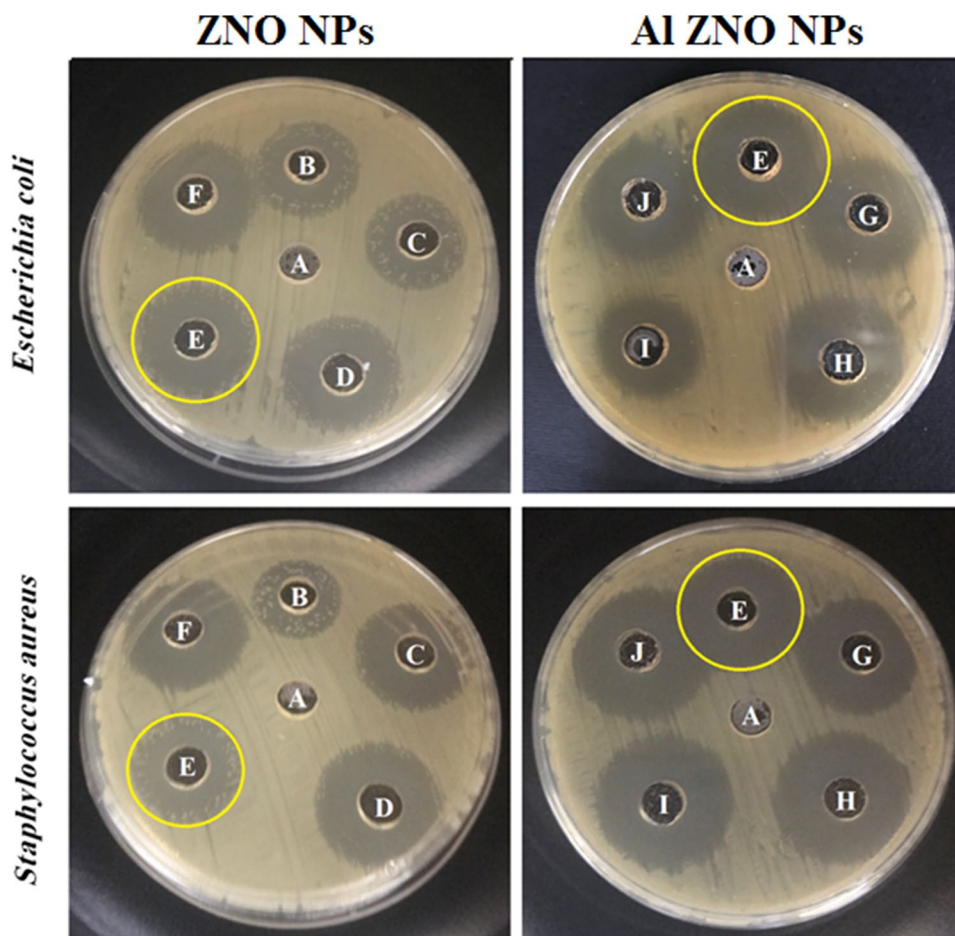
Fig. 8 Optical density (a) and inhibition rate (b) for pathogenic bacteria of *E. coli* and *S. aureus*

activity was observed at highest concentrations (2.66.6 and 333.3 $\mu\text{g mL}^{-1}$), that caused reductions of 17.14% and 11.43%, respectively. Increasing the number of laser pulses in the ablation process exhibited effects on the NPs size, diameter, and morphology, with the increased size or diameter causing adverse impacts on NPs toxicity by decreasing their penetration into the cell membrane. Thus, only few NPs with smaller size can penetrate the membrane and cause cell death. This effect may be attributed to the aggregation and settling of the NPs at the bottom of the tube, with the particle

solution being not able to diffuse properly in the medium [45]. Various factors such as pH, size, ionic strength and capping agent influence the antimicrobial properties of the prepared [46].

Doping with alumina induced a sharp reduction in bacterial growth, with the inhibition rates being in a concentration dependent manner (2.86%, 20.00%, 54.29%, 68.57%). Treatment with Al ZNO NPs against *S. aureus* (orange line) was more effective than that recorded in *E. coli*, showing inhibition rates of 55.22%, 58.20%, 59.70%, 68.66%, respective

Fig. 9 Antibacterial activity of ZNO NPs and Al ZNO NPs against two types of bacteria



to the used concentrations. This can be due to the difference in membrane structures of the bacteria, with regard to the organization of peptidoglycan, which is an essential component in membrane structure and to the mechanism of NPs-bacteria interaction [47]. Table 2 demonstrates the samples of NPs with their respective concentrations, doping ratios, and the used number of pulses.

Figure 9 illustrates the inhibition zone images of ZNO NPs and Al ZNO NPs against the two pathogens. The inhibition zone in *S. aureus* is bigger than that observed in *E. coli* for the same concentrations and conditions. Consistent with the results of bacterial growth in broth, the same picture was drawn on the antibacterial activity performed using well diffusion method. The diameters of inhibition zone for *E. coli* treated with ZNO NPs were 18, 18, 21, 23, and 19 mm whereas those for *S. aureus* were 18, 19, 23, 22.5, and 21 mm (Table 3). These findings showed that *S. aureus* was more sensitive to ZNO NPs than *E. coli*. Similar results, with some alterations, were recorded after treatment with Al ZNO NPs. The diameters of inhibition zone for *E. coli* were 22, 18.5, 21.5, 20 and 23.5 mm, while those for *S. aureus* were 21.5, 20, 23, 26 and 25 mm (Table 3). NPs have a specific property for antibacterial effectiveness against

both Gram positive and Gram negative bacteria, as in the effectiveness of ZNO NPs in preventing the growth of *S. aureus* [10].

The mechanisms of the activity of the nanoparticle might occur in two successive stages; firstly, by causing damages in the outer membrane of the bacterial cell wall through electrostatic or direct interaction between the cell wall the NP. Secondly, by producing an active oxygen environment known as oxidative stress, e.g. during production of H_2O_2 , because of the presence of metal oxides. For example, ZNO NPs shows no effects on the cell shape of *E. coli* O157:H7, but when these particles adhere to the cell surface cell they cause irregular surface structure, membrane bleeding, and outer membrane exhaustion, which causes surface leakage. Thus, the aim behind using NPs as bactericidal agents resides in their bacteriostatic effects; in other words, the effects of ZNO NPs on bacteria can be summarized by their direct interaction, affecting permeability of the outer membrane, causing intracellular oxidative stress, inhibiting cell development, and finally leading to bacterial death [48]. The main steps in the antibacterial activity of these NPs are, first, generation of Zn^{2+} ions which directly affect and damage the cell wall and, second, formation of ROS (reactive oxygen

Table 3 Inhibition zone diameters of *Escherichia coli* and *Staphylococcus aureus*

ZNO NPs			Inhibition zone (mm)	
Sample code	Sample	Mass concentration ($\mu\text{g mL}^{-1}$)	<i>E. coli</i>	<i>S. aureus</i>
A	Control ^a	0	0	0
B	1	66.6	18	18
C	2	133.3	18	19
D	3	200	21	23
E	4	266.6	23	22.5
F	5	333.3	19	21
Al ZNO NPs			Inhibition zone (mm)	
Sample code	Sample	Doping ratio%	<i>E. coli</i>	<i>S. aureus</i>
A	Control ^a	0	0	0
E	4 (E)	266.6 ($\mu\text{g mL}^{-1}$)	22	21.5
G	Al 1	0.2%	18.5	20
H	Al 2	0.27%	21.5	23
I	Al 3	0.33%	20	26
J	Al 4	0.42%	23.5	25

^aControl: deionized distilled water

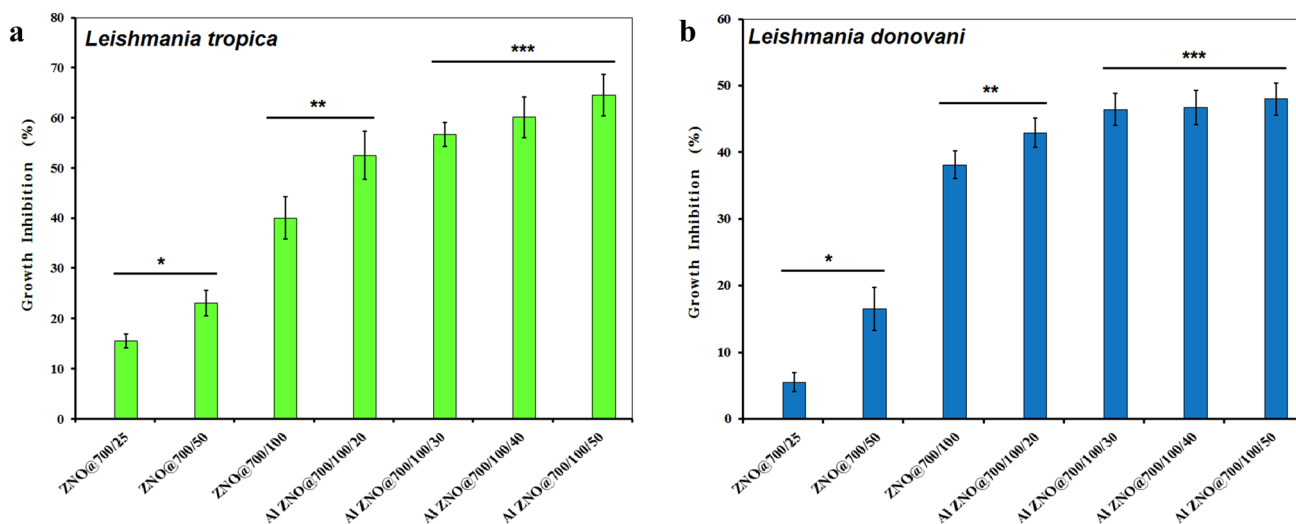


Fig. 10 Growth inhibition of two species of *leishmania* by **a** ZNO NPs and **b** Al ZNO NPs suspension. * $p \leq 0.05$; ** $p \leq 0.01$; *** $p \leq 0.001$

species). Generation of ROS means the production of H_2O_2 and the release of zinc ions in the environment that contains bacteria would facilitate their penetration of the cell wall and exerting their toxicity effects [49].

Figure 10 shows the results of the anti-parasitic activities, as evaluated by the MTT assay, against two species of *Leishmania* (*L. tropica* and *L. donovani*) in the presence of ZNO NPs and Al ZNO NPs in aqueous solution prepared by Nd-Yag laser ablation at a wavelength of 1064 nm with an output power of 700 mJ. As observed in Fig. 10a, ZNO NPs exerted mild cytotoxicity against *L. tropica*, and this effect was concentration dependent. The growth inhibition results

at the first concentration showed a reduction of 15.5% as compared to the non-treated *Leishmania*, while the highest inhibition (40%) was observed at the concentration of $266.6 \mu\text{g mL}^{-1}$. After doping with Al, cell growth exhibited the most remarkable inhibition for all samples (52.5%, 56.6%, 60.1%, and 64.5%).

As shown in Fig. 10b, lower cytotoxic potentials against the *L. donovani* was recorded with the lowest concentration of ZNO NPs (5.5%), followed by the concentration of $133.3 \mu\text{g mL}^{-1}$ (16.5%), and finally the concentration of $266.6 \mu\text{g mL}^{-1}$ (38.1%). With respect to Al ZNO NPs, the samples recorded significant suppression of *L. donovani*

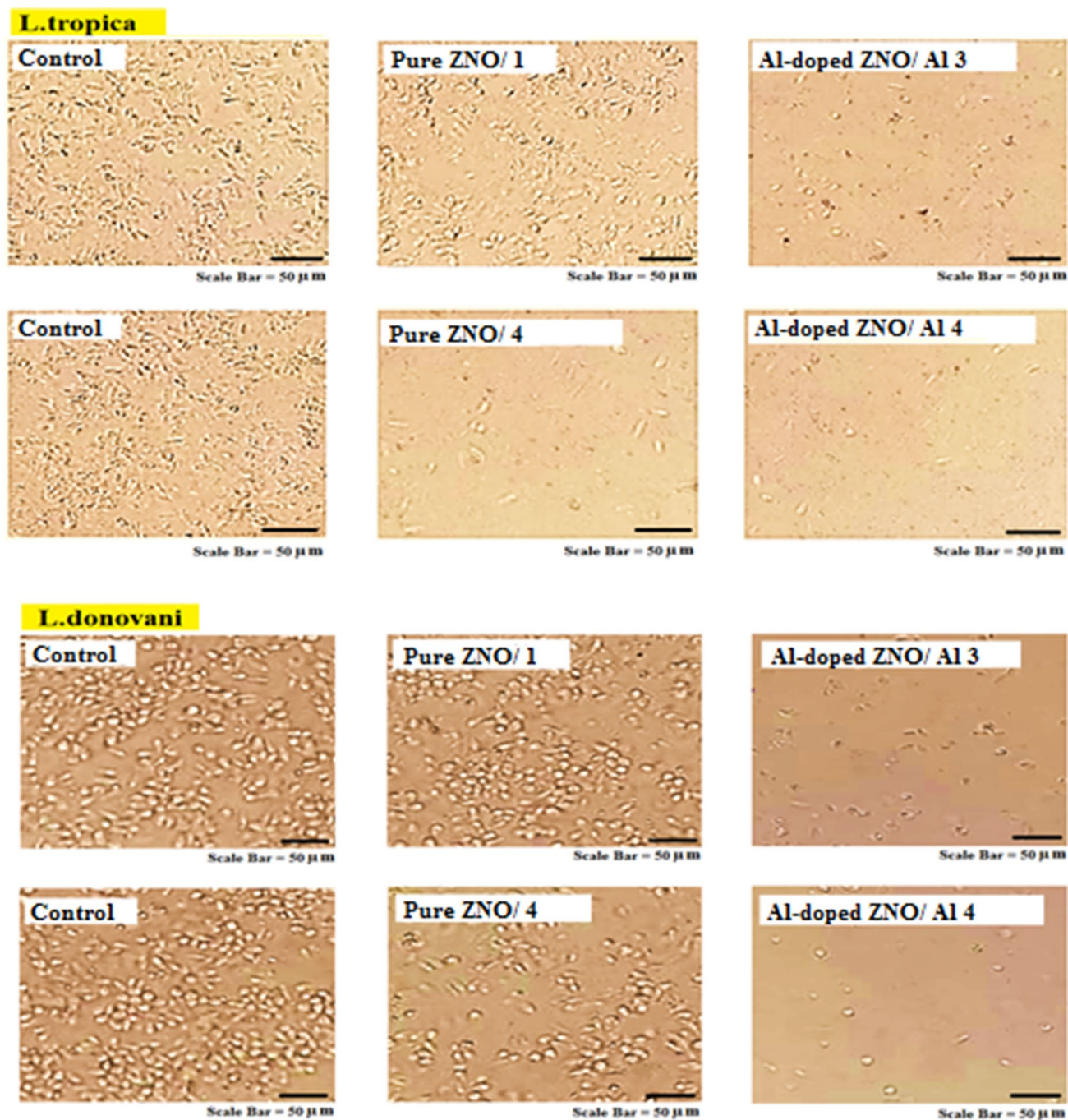


Fig. 11 Micrographic images of cell viability of *L. tropica* and *L. donovani* with two concentrations of pure ZNO NPs (66.6 and $266.6 \mu\text{g mL}^{-1}$) and two concentrations of Al ZNO NPs (0.33 and 0.42%). Control: non-treated cells

growth and the effect was in a concentration dependent manner. The reduction values for the investigated samples were 42.9% , 46.4% , 46.7% , and 48.0% , respective to the used concentrations. These results agree with the observations obtained by our morphological assay on *L. tropica* and *L. donovani* for two different concentrations of pure ZNO NPs and two different doping ratios of Al ZNO NPs

(Fig. 11). The effects of doped NPs were stronger than those of ZNO NPs, while both types of NPs had more potent effects on *L. tropica* than those on *L. donovani*. The exposed cells revealed reduced numbers of viable cells and less morphological changes (Fig. 11). These results demonstrate that ZNO NPs and Al ZNO NPs exert higher and dose-dependent anti-*leishmania* activities due to their

effects on cell viability which are associated with damages to the mitochondrial enzymes and proteins of cell cycle. This higher effectiveness can be also explained by the ability of NPs to generate ROS even in the absence of light that can cause changes in macromolecules such as proteins, nuclei acids, and lipids by effects of oxidative stress. These oxygen species produce free radicals that are short lived and unstable, which influences nuclear viability and

healthiness and finally leads to cell death. ROS can cause oxidation of proteins and peroxidation of lipids that leads to damaging the hardness of the cell membrane, changing permeability of fluids and ion transport, and inhibiting the metabolic processes [50].

Figure 12 shows the anti-cancer activities against MDA-MB-231 cells (human triple-negative breast cancer) as assessed by the MTT method. ZNO NPs exerted a slight activity against MDA-MB-231 cells, and the differences were significant ($p \leq 0.05$) in comparison to the control group. The growth inhibition at the first concentration showed a reduction of 27.5%, while the highest inhibition (43.0%) was observed at the concentration of $266.6 \mu\text{g mL}^{-1}$, comparing with the non-treated cells. After doping with aluminum, cell growth exhibited the most remarkable reduction of MDA-MB-231 cells for all investigated samples. The growth inhibition percentages were 42.8%, 43.0%, 57.0%, and 67.5% and the differences for the higher concentrations were significant ($p \leq 0.001$). This reveals that ZNO NPs and Al ZNO NPs can be useful for the development of anti-cancer drugs including those used for breast cancer therapy. Morphological alterations were examined by subjecting the MDA-MB-231 cells to two different concentrations of ZNO NPs and Al ZNO NPs, as shown in Fig. 13. The results indicated that the cell line was targeted by the NPs which induced numerous morphological alterations, including cell shape changes, cell clumping, and inhibition of cell communication. Al ZNO NPs were more effective against

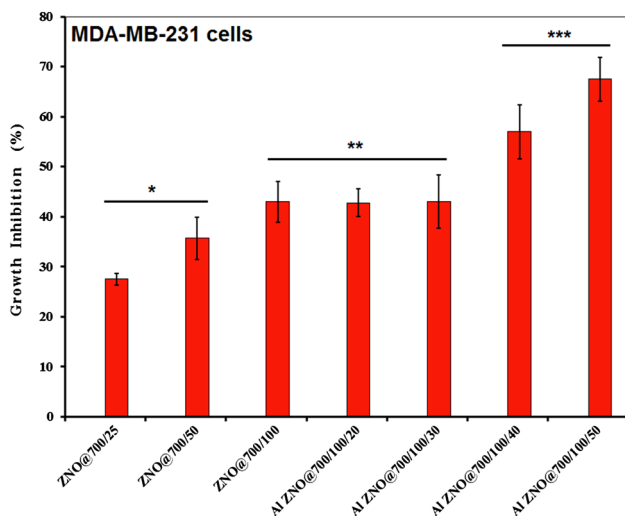


Fig. 12 Anticancer activity for MDA-MB-231 cells treated with ZNO NPs and Al ZNO NPs. * $p \leq 0.05$; ** $p \leq 0.01$; *** $p \leq 0.001$

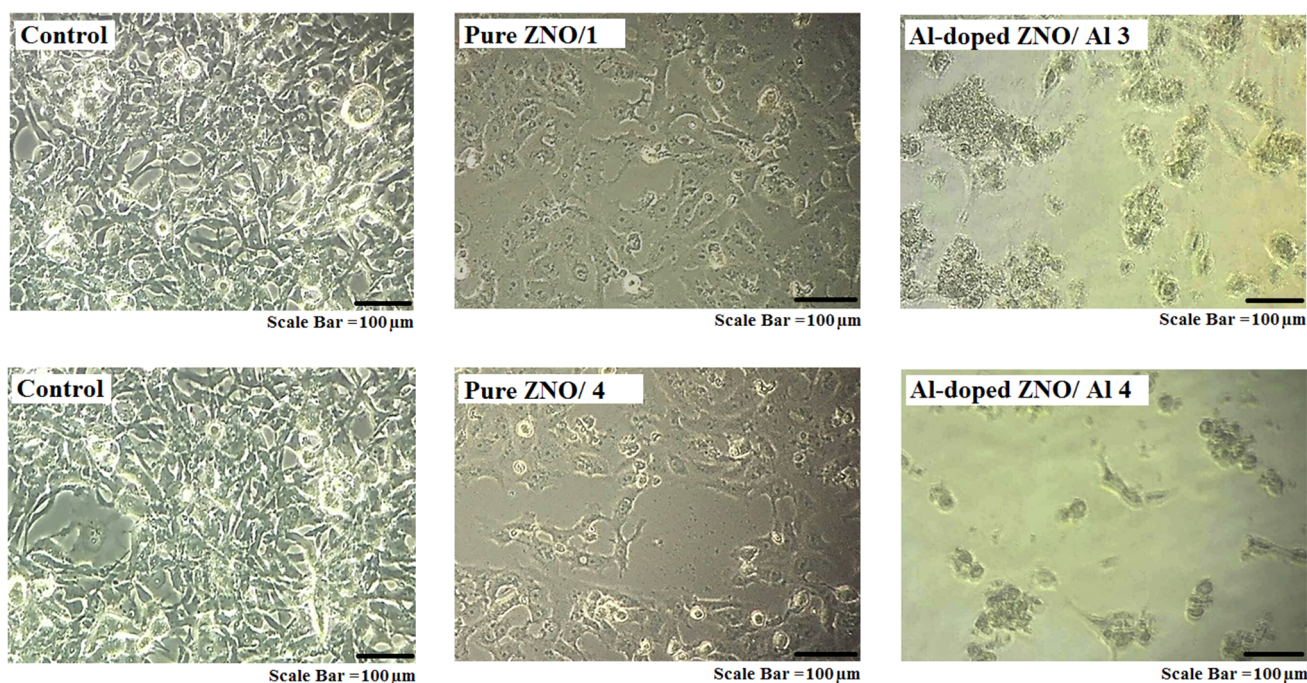


Fig. 13 Micrographic images of MDA-MB-231 cells treated with ZNO NPs and Al ZNO NPs. Two concentrations of ZNO NPs (66.6 and $266.6 \mu\text{g mL}^{-1}$) and two concentrations of Al ZNO NPs (0.33% and 0.42%) were used. Control: non-treated cells

MDA-MB-231 cells; however, no such alterations were observed in non-treated cells. These findings confirm those from a previous study, indicating that Al ZNO NPs had more severe impacts on MCF-7 cells than those of ZNO NPs, without affecting the normal cells [51]. Several mechanisms might cause cancer cell death, including ROS production, antioxidant enzymes inhibition, mitochondrial damage and lipid peroxidation [50].

The mechanisms by which the NPS exerted their toxic effects on MDA-MB231 cells might have included apoptosis, necrosis and generation of ROS; however, the mechanism of cell death in its nanoscale form is not clearly understood and needs more research. In general, the mechanism of action of ZNO NPs and Al ZNO NPs on cancer cells was probably based on the release of dissolved Zn^{2+} ions inside the cells, then increasing ROS actions that caused death of cancer cells by an apoptosis signaling pathway. Zn^{2+} is an anti-cancer agent interfering within the cancer cell and destroying the mitochondrial electron transport chain with realizing a huge amount of ROS that cause mitochondrial damage, loss of protein activity balance, and apoptosis [51]. Introduction of the transition metal ion (Al^{3+}) into a ZNO crystal lattice causes an increase in the ability of particles to generate ROS. This effect is attributed to the breadth in band gap energy which causes a stronger catalysis of the separation of H_2O_2 molecules into hydroxide ions and fundamental hydroxyl groups or into hydrogen ions and hydroperoxy radicals. Such an influence results in the enhancement of the protein oxidation and redox state inside the cells and finally leads to the killing of cancer cells [52]. Thus, the cells death obtained in the present results allow us to predict that their potential is not only because of the cytotoxic effect, but also in terms of the potential for tumor reduction.

4 Conclusions

The ZNO and Al ZNO NPs were prepared using pulsed laser ablation in liquid and their physical and biomedical properties were studied. From the present study, we conclude that Al ZNO NPs were successfully synthesized, showing a hexagonal structure with high absorption in the UV region. The FSEM imaging revealed more modification in the structures of these NPs with increasing the doping ratio. The prepared Al ZNO NPs showed a strong antibacterial potential against the tested pathogenic bacteria. Additionally, the MTT assay confirmed their cytotoxic activity against different leishmania species, as well as promising anticancer potential against MDA-MB231 cells. The current study importantly demonstrates the possible usefulness of the synthesized NPS in the development of therapies against cancer in general and breast cancer in particular.

Compliance with Ethical Standards

Conflict of interest No potential conflict of interest was reported by the authors.

References

- H.F. Chen, B.H. Clarkson, K. Sun, J.F. Mansfield, *Colloids. Interface Sci.* **288**, 97 (2005)
- Y. Liu, J. Zhan, M. Ren, K. Tang, W. Yu, Y. Qian, *Mater. Res. Bull.* **36**, 1231 (2001)
- J. Singh, T. Dutta, K.H. Kim, M. Rawat, P. Samddar, P. Kumar, *J. Nanobiotechnol.* **16**, 84 (2018)
- E. Sahin, S.J. Musevi, A. Aslani, *Arabian J. Chem.* **10**, S230 (2017)
- N.L. Hussein, K.S. Khashan, H.M. Rasheed, H.Y. Hammoud, R.M.S. Al-Haddad, *Iraq. J. Sci.* **56**, 1129–1143 (2019)
- K.S. Khashan, S.F. Abbas, *Int. J. Nanosci.* **18**, 1850021 (2019)
- J. Singh, V. Kumar, K.H. Kim, M. Rawat, *Environ. Res.* **177**, 108569 (2019)
- J. Singh, S. Kaur, G. Kaur, S. Basu, M. Rawat, *Green Process. Synth.* **8**, 280 (2019)
- G. Singh, J. Singh, S.S. Jolly, R. Rawat, D. Kukkar, S. Kumar, S. Basu, M. Rawat, *J. Mater. Sci. Mater. Electron.* **29**, 7371 (2018)
- H. Mirzaei, M. Darroudi, *Ceram. Int.* **43**, 914 (2017)
- Y. Liu, L. He, A. Mustapha, H. Li, Z.Q. Hu, M. Lin, *J. Appl. Microbiol.* **107**, 1193 (2009)
- V. Saxena, P. Chandra, L.M. Pandey, *Appl. Nanosci.* **2018**, 8 (1925)
- J. Singh, A. Rathi, M. Rawat, V. Kumar, K.H. Kim, *Comp. Part B. : Eng.* **166**, 370 (2019)
- K.S. Khashan, M. Mahdi, *Appl. Nanosci.* **7**, 589 (2017)
- K.S. Khashan, F. Mahdi, *Surf. Rev. Lett.* **24**, 1750101 (2017)
- K.S. Khashan, A.I. Hassan, A.J. Addie, *Surf. Rev. Lett.* **23**, 1650044 (2016)
- P. Banerjee, W.J. Lee, K.R. Bae, S.B. Lee, G.W. Rubloff, *J. Appl. Phys.* **108**, 043504 (2010)
- A.N.P. Madathil, K.A. Vanaja, M.K. Jayaraj, *Nanophotonic Materials IV* **6639**, 66390J (2007)
- K.P. Singh, U. Timilsina, H.K. Tamang, S. Thapa, A.J. Agarwal, *Nepal Assoc. Med. Lab. Sci.* **11**, 54 (2012)
- M.M. Chikkanna, S.E. Neelagund, K.K. Rajashekarappa, *SN Appl. Sci.* **1**, 117 (2019)
- M.R.A. Bhuiyan, M.M. Alam, M.A. Momin, H. Mamur, *Inter. J. Energy Appl. Technol.* **4**, 33 (2017)
- K. Singh, J. Singh, M. Rawat, *SN Appl. Sci.* **1**, 624 (2019)
- K.S. Khashan, G.M. Sulaiman, R. Mahdi, *Artif. Cells Nanomed. Biotechnol.* **45**, 1699 (2017)
- K.S. Khashan, G.M. Sulaiman, A.H. Hamad, F.A. Abdulameer, A. Hadi, *Appl. Phys. A* **123**, 190 (2017)
- K.S. Khashan, M.S. Jabir, F.A.J. Abdulameer, *Phys. Conf. Series* **1003**, 012100 (2018)
- R. Hameed, K.S. Khashan, G.M. Sulaiman, *Mater. Today Proceed.* **20**, 539 (2020)
- R.A. Ismail, K.S. Khashan, M.F. Jawad, A.M. Mousa, F. Mahdi, *Mater. Res. Exp.* **5**, 055018 (2018)
- J.S. Duque, B.M. Madrigal, H. Riascos, Y.P. Avila, *Coll. Interf.* **3**, 25 (2019)
- M.M.F. Al-Halbosiy, Z.A. Thabit, S.A.D.A.S. Al-Qaysi, T.A.A. Moussa, *Baghdad Sci. J.* **15**, 238 (2018)
- Z.K. Taha, S.N. Hawar, G.M. Sulaiman, *Biotechnol. Lett.* **41**, 899 (2019)

31. S.I. Dolgaev, A.V. Simakin, V.V. Voronov, G.A. Shafeev, F. Bozon-Verduraz, *Appl. Surf. Sci.* **186**, 546 (2002)
32. R. Mahfouz., F.J. Cadete Santos Aires, A. Brenier, B. Jacquier, J.C. Bertolini, *Appl. Surf. Sci.* **354**, 5181 (2008)
33. M.A. Batista, A.C.S.D. Costa, I.G.D. Souza Junior, J.M. Bigham, *Rev. Bras. Ciênc. Solo* **32**, 561 (2008)
34. A. Rajalaxshmi, J.J. Clara, *Eur. J. Phar. Med. Res.* **4**, 712 (2017)
35. M.S. Khalaf, A.H. Mohammed, S.S. Shaker, *Eng. Technol. J.* **36**, 93 (2018)
36. K. Gherab, Y. Al-Douri, C.H. Voon, U. Hashim, M. Ameri, A. Bouhemadou, *Res. Phys.* **7**, 1190 (2017)
37. M. Vadivel, R.R. Babu, K. Ramamurthi, *Int. J. Chem. Tech. Res.* **7**, 1206 (2014)
38. K.I. Hassoon, S.H. Sabeeh, M.A.J. Khalaf, Al-Nahrain. *Univ. Sci.* **20**, 70 (2017)
39. R.A. Ismail, A.K. Ali, M.M. Ismail, K.I. Hassoon, *Appl. Nanosci.* **1**, 45 (2011)
40. N. Krstulovic, K. Salamon, O. Budimljija, J. Kovac, J. Dasovic, P. Umek, I. Capan, *Appl. Surf. Sci.* **440**, 916 (2018)
41. A. Alkahlout, D.N. Al, I. Grobelsek, M. Jilavi, P.W.J. De Oliveira, *Materials* **2014**, 235638 (2014)
42. M. Kumar, B. Singh, P. Yadav, V. Bhatt, M. Kumar, K. Singh, A.C. Abhyankar, A. Kumar, J.H. Yun, *Ceram. Int.* **43**, 3562 (2017)
43. A.A. Al-Ghamdi, O.A. Al-Hartomy, M. El Okr, A.M. Nawar, S. El-Gazzar, T.F. El-, F. Yakuphanoglu, *Spectrochim. Acta A Mol. Biomol. Spectrosc.* **131**, 512 (2014)
44. X. Li, L. Wang, Y. Fan, Q. Feng, F.Z. Cui, *J. Nanomater.* (2012). <https://doi.org/10.1155/2012/548389>
45. J.K. Patra, K.H. Baek, *J. Nanomater.* **2014**, 219 (2014)
46. D.M. Aruguete, M.F. Hochella, *Environ. Chem.* **7**, 3 (2010)
47. Y. Xie, Y. He, P.L. Irwin, T. Jin, X. Shi, *Appl. Environ. Microbiol.* **77**, 2325 (2011)
48. S. Liu, Y. Lai, X. Zhao, R. Li, F. Huang, Z. Zheng, M. Ying, *Mater. Res. Express* **6**, 0850c6 (2019)
49. L. Salazar, M.J. Vallejo Lopez, M. Grijalva, L. Castillo, A. Maldonado, *J. Nanotechnol.* **6**, 1 (2018)
50. M.J. Akhtar, H.A. Alhadlaq, A. Alshamsan, M.M. Khan, M. Ahamed, *Sci. Rep.* **5**, 13876 (2015)
51. J. Jiang, J. Pi, J. Cai, *Bioinorg. Chem. Appl.* **2018**, 1062562 (2018)
52. J.W. Rasmussen, E. Martinez, P. Louka, D.G. Wingett, *Expert. Opin. Drug Deliv.* **7**, 1063 (2010)

Publisher's Note Springer Nature remains neutral with regard to jurisdictional claims in published maps and institutional affiliations.